Neuro-Oncology

Neuro-Oncology 2015; **0**, 1–11, doi:10.1093/neuonc/nov106

pH-weighted molecular imaging of gliomas using amine chemical exchange saturation transfer MRI

Robert J. Harris, Timothy F. Cloughesy, Linda M. Liau, Robert M. Prins, Joseph P. Antonios, Debiao Li, William H. Yong, Whitney B. Pope, Albert Lai, Phioanh L. Nghiemphu, and Benjamin M. Ellingson

Department of Radiological Sciences (R.J.H., W.B.P., B.M.E.), Department of Biomedical Physics (R.J.H., B.M.E.), Department of Neurology (T.F.C., A.L., P.L.N.), Department of Neurosurgery, David Geffen School of Medicine, University of California Los Angeles, Los Angeles, California (L.M.L., R.M.P., J.P.A.); Department of Biomedical Sciences and Imaging, Cedars-Sinai Medical Center, Los Angeles, California (D.L.); Department of Bioengineering (D.L., B.M.E.), Department of Pathology and Laboratory Medicine, David Geffen School of Medicine, University of California Los Angeles, Los Angeles, California (W.H.Y.)

Corresponding Author: Benjamin M. Ellingson, PhD, Assistant Professor of Radiology, Biomedical Physics, and Bioengineering, Department of Radiological Sciences, David Geffen School of Medicine, University of California – Los Angeles, 924 Westwood Blvd, Suite 615, Los Angeles, CA 90024 (bellingson@mednet.ucla.edu).

Background. Interstitial tissue acidosis resulting from abnormal perfusion and metabolism is a hallmark of cancer. The current study demonstrates that chemical exchange saturation transfer (CEST) MRI can be used as a noninvasive pH-weighted molecular imaging technique by targeting the chemical exchange between amine protons and protons in extracellular bulk water.

Methods. First, the sensitivity of amine CEST was validated in phantoms under a variety of conditions, including different magnetic field strengths, amino acid concentrations, and pH values. Amine CEST was compared with histology in both a preclinical GL261 intracranial glioma model at 7T and human patients at 3T. The association between physiologic and pH-weighted MRI was explored, along with the ability to predict time to progression to radiochemotherapy in 20 glioblastoma patients.

Results. *z*-Spectral asymmetry increased at 3 ppm (amine range) on CEST MRI with decreasing pH within the range observed in tumors for both 3T and 7T scanners. Lesions with acidic signatures showed active tumor and pseudopalisading tumor on histology and showed elevated FDOPA PET uptake, lactate on MR spectroscopy, and perfusion abnormalities. Patients with acidic lesions after surgery or stable/growing acidic lesions had a shorter time to progression following radiochemotherapy compared with patients with lesions demonstrating relatively low acidity ($P < .001$).

Conclusion. Results suggest pH-weighted MRI may provide new insight into brain tumor physiology beyond traditional imaging technologies.

Keywords: CEST, chemical exchange saturation transfer, glioma, pH, pH-weighted MRI.

Tissue acidosis contributes directly to a microenvironment hospitable to cancer. Various studies have reported that tumor cells have alkaline intracellular pH values (7.1–7.6 compared with 7–7.2 in normal tissues) and acidic extracellular pH values (6.2–6.9 compared with 7.3–7.4 in normal tissues).[1] This decrease in extracellular pH is thought to be directly due to tumor size[2] and altered blood flow,[3] leading to increased hypoxia. This lack of oxygen increases glycolysis[4] and results in accumulation of carboxylic acid[5] and/or lactic acid[6] in the extracellular space (Fig. 1A). Additionally, active transport of protons out of tumor cells to maintain high intracellular pH results in further decreases in pH within the immediate environment. These effects are further exacerbated by a diminished buffering capability of tumor interstitial fluid along with limited elimination of lactic acid and protons into the blood vasculature.

This increase in extracellular acidity comes with dramatic consequences (Fig. 1A), as it can be directly linked to the degree of tumor aggressiveness. A decrease in extracellular pH results in decreased immune function,[7] increased chromosomal rearrangements,[8] increased tumor invasion,[9] and increased angiogenesis through elevated vascular endothelial growth factor[10] and platelet-derived endothelial cell growth factor.[11] The decrease in extracellular pH also results in resistance to various

Received 3 March 2015; accepted 25 May 2015

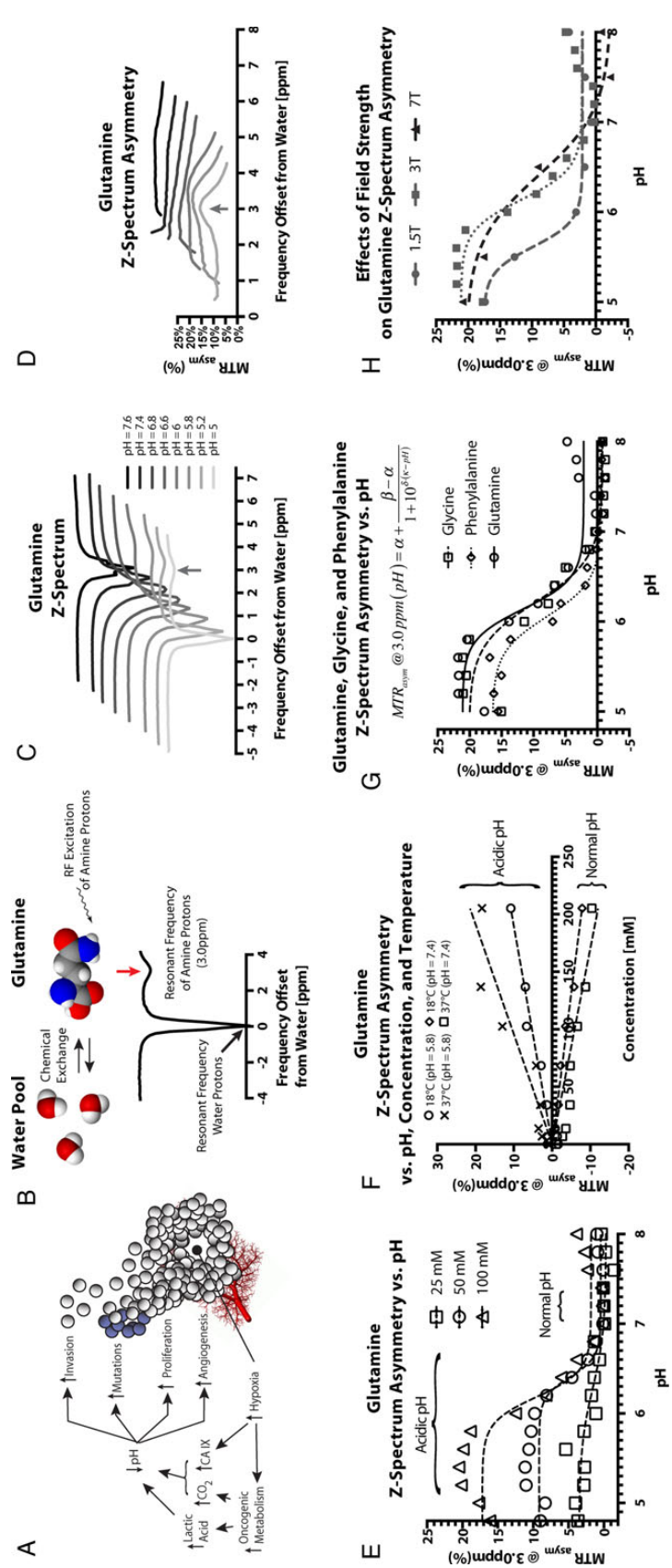

Fig. 1. Phantom and preclinical results for pH-weighted molecular MRI using CEST imaging targeting amine protons on glutamine. (A) Tumor growth results in increased hypoxia and increased expression of carbonic anhydrase 9 (CA IX), which enhances extracellular acidification through catalyzing CO_2 into carboxylic acid and protons in solution. Oncogenic metabolism further decreases extracellular pH through increased lactic acid via the Warburg effect. This decrease in pH directly increases tumor invasion, the number of mutations, proliferation rate, and angiogenesis. (B) pH-weighted MRIs are obtained by exploiting the CEST effect, or off-resonance (+3.0 ppm) radiofrequency saturation of amine protons on glutamine (and other amino acids) undergoing chemical exchange with the bulk water pool. (C) The CEST *z*-spectra for glutamine phantoms (100 mM) and various pH. (D) The MTR_{asym} of the CEST *z*-spectrum showing increased asymmetry with decreasing pH at 3T. (E) Glutamine *z*-spectrum asymmetry, MTR_{asym} (3.0 ppm), obtained from the *z*-spectrum of glutamine phantoms at various pH and concentrations. (F) Glutamine *z*-spectrum asymmetry, MTR_{asym}(3.0 ppm), for different pH, concentration, and temperature. (G) CEST *z*-spectrum asymmetry, MTR_{asym}(3.0 ppm) for glutamine, glycine, and phenylalanine phantoms (100 mM) as a function for pH. (H) CEST *z*-spectrum asymmetry, MTR_{asym}(3.0 ppm) for glutamine (100 mM) for magnetic field strengths of 1.5T, 3T, and 7T. (I) Postcontrast T1-weighted, T2-weighted, and pH-weighted MRIs for C57BL/6 control animals inoculated with PBS. (J) Postcontrast, T2-weighted, and pH-weighted MRIs for GL261 inoculated C57BL/6 mice. (K) H&E stain of the control C57BL/6 mouse. (L) H&E stain of the GL261 tumor. (M) MTR_{asym} (3.0 ppm) was significantly higher within the T2 hyperintense lesion compared with contralateral brain in $n = 9$ mice with GL261 tumors (paired *t*-test, $P = .0002$).

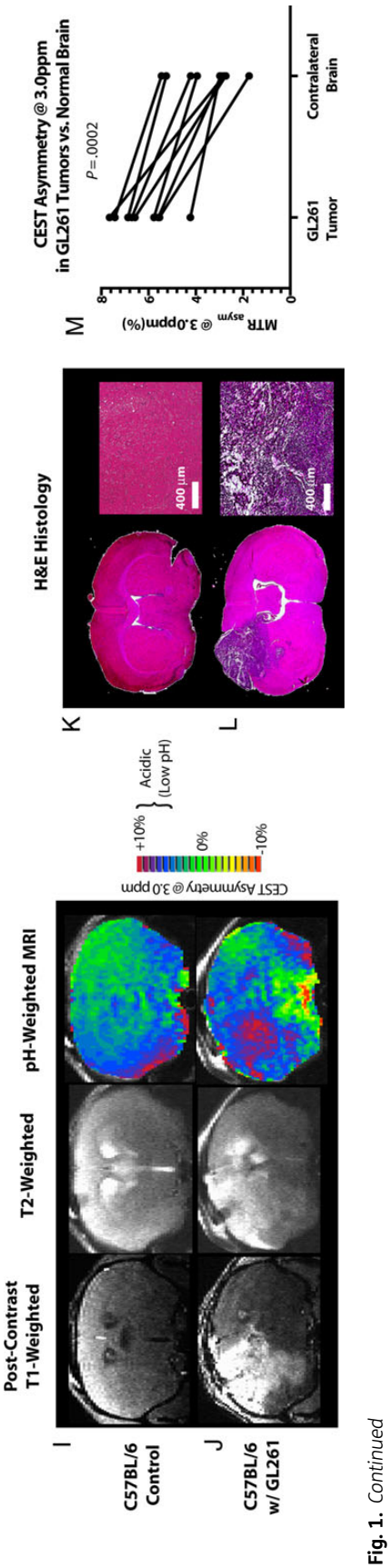

Fig. 1. *Continued*

forms of therapy, including resistance to radiation therapy[12] and specific chemotherapies.[13] Thus, a noninvasive imaging method for spatially identifying regions of low tissue pH may be invaluable for early identification of malignant transformation, predicting early treatment resistance, as well as potentially detecting early tumor invasion, proliferation, angiogenesis, hypoxia, genetic mutations, and altered immune response.

The chemical exchange between amine and amide protons in bulk water has been shown to be pH dependent using a new imaging method called chemical exchange saturation transfer (CEST) imaging.[14] As the hydrogen ion activity in a solution changes, the chemical exchange rate between proton groups will change as well, which will affect the properties of CEST contrast. Since glutamine and other amino acids contain an amine and an amide group having different chemical shift frequencies (2.8–3.0 ppm and 3.5 ppm, respectively, compared with water protons) and the concentrations of mobile glutamine and other neutral amino acids are elevated in regions of active tumor because they are a major source of fuel for malignant tumors[15,16] and transport systems are often amplified to increase glutamine consumption,[17] we hypothesized that CEST imaging targeting amine protons on glutamine would provide a higher CEST contrast at 2.8–3.0 ppm (Fig. 1B) and result in a novel imaging biomarker for mapping regions of low pH which may be specific to viable tumor microenvironments. The elevated levels of amino acids in areas of active tumor should serve to amplify, rather than dilute, the CEST contrast in regions of low pH. In the current study, we demonstrate that the amine proton CEST signal increases with increasing amino acid concentration and decreasing pH, and that this pH-weighted molecular MRI technique can be used to provide new insight into brain tumor physiology and behavior beyond traditional structural and functional imaging technologies.

Methods

Chemical Exchange Saturation Transfer MRI Theory

CEST MRI is sensitive to the chemical exchange between exchangeable protons on metabolite functional groups (eg, hydroxyls, amides, amines) through nuclear magnetic resonance (NMR) saturation of these protons using radiofrequency excitation with frequencies off-resonance from bulk mobile water protons, and then measuring the indirect effects on the mobile water NMR signal traditionally used for MRI. As off-resonance excitation and the resulting saturation of the mobile water pool can arise due to a number of factors, including magnetization transfer from the semisolid macromolecular pool and spillover effects from bulk water excitation, CEST data for each image voxel are analyzed by calculating the magnetization transfer ratio asymmetry (MTR_{asym}) as given by:

$$MTR_{asym}(\Delta\omega) = \frac{S_{sat}(-\Delta\omega) - S_{sat}(-\Delta\omega)}{S_0} \qquad (1)$$

where $S(\Delta\omega)$ and $S(-\Delta\omega)$ are the magnitude of the MR signal acquired using an irradiation frequency $\Delta\omega$ or $-\Delta\omega$ from water (referenced at 0 ppm), and S_0 is the MR signal acquired using no off-resonance saturation pulse used for normalization. All calculations were performed on a voxel-by-voxel basis. For

the CEST experiment, a series of MR images were acquired using a range of off-resonance irradiation frequencies, producing a "z-spectrum," represented by the function $MTR_{asym}(\Delta\omega)$ for each image voxel. The resulting pH-weighted molecular MR images were then generated by calculating $MTR_{asym}(3.0\ ppm)$, targeting the amine protons on glutamine or other neutral amino acids.

Phantom Preparation

In order to determine the dependence of glutamine CEST on pH and concentration, we prepared 50-mL samples of 25 mM, 50 mM, and 100 mM glutamine in distilled water. For each concentration, 24 samples at different pH varying from 4.0 to 8.6 in intervals of 0.2 were created by titrating 0.1 M HCl or NaOH and using a pH meter accurate to 0.1 pH units. In order to demonstrate that this effect is similar for other neutral amino acids, we prepared a similar set of samples using 100 mM glycine dissolved in distilled water at pH values 4.0–8.6 in units of 0.2, and a set of samples with 100 mM phenylalanine dissolved in distilled water at pH values 4.0–8.6 in units of 0.2.

Phantom Imaging

Due to the large number of samples evaluated, each set of 24 vials with various pH values was split into 3 scans of 8 samples each. The samples were held stationary in a bath of room-temperature water (21°C). For each set of samples, 51 z-spectral points were acquired from −5.0 ppm to +5.0 ppm in units of 0.2 ppm. Schmitt and colleagues[18] previously demonstrated that when pulsed-wave saturation is necessary, as is the case with clinical imaging where radiofrequency energy deposition is limited for safety, pulses of 100 ms at 50% duty cycle generate maximum contrast in CEST experiments. Therefore, a saturation pulse train consisting of fifteen 100-ms pulses (50% duty cycle) at an amplitude of $B1 = 2.0\ \mu T$ was applied, followed by a 90-degree excitation pulse and gradient echo readout. Other parameters are included in the Supplementary Materials.

Scan times were restrained clinically, necessitating a reduction in the saturation pulse train length during collection of clinical patient data. The final clinical protocol was based on empirical data (not shown) suggesting that a train length of five 100-ms radiofrequency pulses with 50% duty cycle and amplitude of 5 μT will result in 85%–95% maximum saturation at 3.0 ppm when evaluated using 100 mM glutamine at pH = 5. Additionally, we explored the CEST effects for various field strengths using a 1.5T Siemens Avanto human MR scanner, a 3T Siemens Trio human MR scanner, and a 7T Bruker Biospec preclinical MR scanner.

Animal Preparation

To test the efficacy of glutamine CEST as a pH-weighted biomarker using a preclinical 7T small animal MR scanner, female C57BL/6 mice (6–8 wk of age) were evaluated. One C57BL/6 mouse was injected with phosphate buffered saline (PBS; control) while 9 C57GL/6 mice were injected with 2×10^6 GL261 glioma cells and allowed to grow for 14 days. All procedures and protocols used in the current study were approved by the UCLA Institutional Animal Care and Use Committee to ensure proper animal care.

μMR Acquisition

Mice were sedated with 1%–3% isoflurane under O_2/N_2 flow, and respiration was monitored. Mice were kept warm with water heated to 37°C circulated using a TP500 water pump (Gaymar Solid State). All images were acquired on a 7T Bruker Biospec system with a custom-built 2.2-cm RF birdcage coil. Each mouse was scanned <1 h. We collected a series of anatomical images as well as pH-weighted MR images in these mice. Pre- and postcontrast 3D T1-weighted anatomical images were collected using a 3D fast low flip angle acquisition technique. Prior to contrast administration, pH-weighted CEST images were collected using a 2D gradient echo acquisition technique. Total CEST scan time was 10.5 min.

Human Patients

A total of 25 patients with histologically confirmed primary gliomas (World Health Organization [WHO] grades II–IV) were enrolled in this prospective clinical trial funded by the National Institutes of Health, compliant with the Health Insurance Portability and Accountability Act, and approved by the institutional review board at our institution. A total of 3 patients received CEST imaging, single-voxel MR spectroscopy and 6-[18F] fluoro-L-dopa (^{18}F-FDOPA) PET imaging within 1 month for direct comparison; 2 patients received stereotactic pH-image–guided biopsies (a suspected low-grade glioma and a suspected recurrent glioblastoma); and 20 patients with histologically confirmed glioblastoma were evaluated at 3 time points—(i) baseline: postsurgical and prior to radiochemotherapy; (ii) midtreatment: ∼3 weeks after the start of radiochemotherapy; and (iii) posttreatment: ∼6–10 weeks after the start of radiochemotherapy, or 0–4 weeks after completion of concurrent radiation and chemotherapy. All glioblastoma patients evaluated underwent maximal surgical resection followed by standard treatment with radiotherapy and concurrent temozolomide. Follow-up scans were also obtained in these patients for comparison and radiographic response as determined by the Response Assessment in Neuro-Oncology criteria.[19]

Clinical 3T Imaging

Standard anatomic MRI

All patients underwent standard clinical MRI on a 3T MR system (Siemens 3T Trio) that included pre- and postcontrast (gadolinium [Gd] diethylenetriamine pentaacetic acid [DTPA] at a dose of 0.1 mmol/kg body weight; Magnevist) axial T1-weighted magnetization prepared rapid gradient echo (MPRAGE), axial T2-weighted, and axial fluid-attenuated inversion recovery (FLAIR) sequences.

Physiologic imaging

In addition to structural MRI, patients received 64 direction diffusion tensor imaging (DTI), dynamic susceptibility contrast

(DSC) perfusion MRI and single-voxel NMR spectroscopy (see Supplementary Materials). Prior to DSC-MRI acquisition, a 0.025 mmol/kg pre-load dose of Gd contrast agent was administered to diminish the T1 effects of contrast agent extravasation.[20] A 3- to 5-cc/s bolus of Gd-DTPA, administered at a dose of 10–20 cc (0.075 mmol/kg), was used in the acquisition of DSC as well as the subsequent postcontrast T1-weighted images (total of 0.1 mmol/kg). Parametric maps of cerebral blood volume (CBV) and cerebral blood flow (CBF) were calculated using commercially available postprocessing software (IB Neuro v2.0, Imaging Biometrics) including contrast leakage correction.[21] DTI and DSC-MRI were only used for qualitative comparison in some patients for this study. Single-voxel NMR spectroscopy was performed at 3T using a standard point resolved spectroscopy sequence with short echo (30 ms).

Clinical pH-weighted CEST imaging

A total of 1 to 5 slices of CEST images with varying *z*-spectral points ranging from 5 to 51 and from −5.0 ppm to +5.0 ppm were acquired in clinical patients. A radiofrequency saturation pulse train of three 100-ms pulses (50% duty cycle) at B1 = 6.0 μT was applied, followed by a 70-degree excitation pulse and gradient echo readout. For biopsy patients, 3 slices were acquired through the largest extent of the tumor using spectral points acquired at 0, ±0.125, ±0.25, ±0.375, ±0.5, ±2.5, ±2.75, ±3.0, ±3.25, and ±3.5 ppm, rather than a full *z*-spectrum with a single slice. All other CEST scan parameters are in Supplementary Materials.

CEST Postprocessing and Analysis

All CEST data were motion corrected and inhomogeneity corrected prior to analysis. Motion correction was performed using the *mcflirt* function in FMRIB Software Library (Functional Magnetic Resonance Imaging of the Brain; http://www.fmrib.ox.ac.uk/fsl/). Inhomogeneity correction consisted of defining the lowest-intensity point in the *z*-spectrum of each voxel as the central water frequency and shifting the other data points in that voxel's *z*-spectrum accordingly.[22] For the phantom experiments, a circular region of interest was drawn on each sample and the mean value for each spectral point was calculated to obtain the average *z*-spectra for a sample. MTR_{asym} at 3.0 ppm was calculated from these *z*-spectra for each sample. For each patient, the postcontrast T1-weighted image and CEST data were registered and interpolated to the resolution of the T2-weighted FLAIR images. Voxelwise maps of MTR_{asym} at 3.0 ppm were calculated from the CEST data.

In order to test whether there was a difference in MTR_{asym} at 3.0 ppm as a function of pH between three neutral amino acids (glycine, glutamine, and phenylalanine), we applied the simple competitive inhibitor equation:

$$MTR_{asym}@3.0\,\text{ppm}\,(\text{pH}) = \alpha + \frac{\beta - \alpha}{1 + 10^{\delta(\kappa - \text{pH})}} \qquad (2)$$

where α is the MTR_{asym} at 3.0 ppm for high pH environments, β is the MTR_{asym} at 3.0 ppm for low pH environments, δ is the sensitivity of MTR_{asym} at 3.0 ppm to changes in pH, and κ is the pH required for 50% of the maximum span in MTR_{asym} measurements at 3.0 ppm between high and low pH limits.

6-[18F] Fluoro-L-Dopa Positron Emission Tomography

A subset of patients ($n = 3$ with matching MR spectroscopy and $n = 2$ biopsy patients) received ^{18}F-FDOPA PET to scans to confirm the presence of metabolically active tumor. ^{18}F-FDOPA PET scans were acquired using a high-resolution full-ring PET scanner (ECAT-HR; CTI/Mimvista). Patients were instructed to fast for more than 4 h prior to PET acquisition. ^{18}F-FDOPA was synthesized and injected intravenously, injected doses averaging 125.4 ± 22.9 MBq, 1.54 ± 0.37 Bq/kg. A CT scan was acquired prior to PET for attenuation correction. 3D ^{18}F-FDOPA emission data were acquired 10 min after radiotracer injection for a total of 30 min. Data were integrated between 10 and 30 min from injection to obtain 20-min static ^{18}F-FDOPA images following reconstruction. PET images were reconstructed using an ordered-subset expectation maximization iterative reconstruction algorithm consisting of 6 iterations with 8 subsets.[23,24] Lastly, a Gaussian filter with a full width at half maximum of 4 mm was applied. Uptake levels were normalized to the basal ganglia to highlight areas of abnormal ^{18}F-FDOPA uptake in the tumor.

Stereotactic Image–Guided Biopsies and Tissue Processing

Stereotactic pH-image–guided biopsies were performed in 2 patients. Each patient's pH-weighted image was overlaid on the postcontrast MPRAGE image for localizing of targets. When no enhancing lesion was present, T2/FLAIR images were used for target localization. The first patient was a suspected low-grade glioma biopsy patient. One region of elevated CEST contrast consistent with low pH and one region of low CEST contrast consistent with normal pH were biopsied. Standard hematoxylin and eosin (H&E) staining was performed as well as immunohistochemistry staining for Ki-67 expression. Sections of 5 microns were cut from formalin-fixed paraffin-embedded samples and processed for immunohistochemical detection of Ki-67 (Clone VP-RM04, rabbit monoclonal, 1:100 dilution, Vector Laboratories). Appropriate positive and negative controls were used to ensure good immunohistochemical staining. The second patient was a glioblastoma patient with suspected recurrence. Two regions of elevated CEST contrast consistent with acidic tissue and one region with low CEST contrast were biopsied, then H&E staining was performed and reviewed by a board certified neuropathologist blinded to the specific targets.

Comparison of Progression-Free Survival After Radiochemotherapy in Acidic Versus Non-Acidic Glioblastoma

In order to assess whether tumors with low pH signatures on CEST at baseline were more likely to have a shorter PFS after treatment with radiochemotherapy, we scored each tumor based on the amount of elevated CEST signal at 3.0 ppm. In particular, we defined "acidic" lesions as containing a

substantial proportion (>50%) of positive CEST asymmetry at 3.0 ppm within areas of contrast enhancement and/or T2 or FLAIR hyperintensity. Alternatively, patients were scored as having "non-acidic" lesions if a significant portion of the lesion did not show an elevated CEST signal. Next, we subjectively scored each lesion as "increasing" or "stable/decreasing" on pH-weighted MR scans before, during, and after radiochemotherapy in order to determine whether changes in the acidic lesion size could be used as an early response metric. Log-rank tests on Kaplan–Meier data were used to describe differences in progression-free survival (PFS) between these patient groups.

Results

The CEST *z*-spectrum in pH-varying samples containing glutamine illustrated reduced normalized signal intensity of the bulk water pool ($S(\omega)/S_0$) during off-resonance irradiation around 3.0 ppm (Fig. 1C), and asymmetry of the *z*-spectrum (MTR_{asym}) increased with decreasing pH of glutamine solution (Fig. 1D), which is consistent with the expected CEST contrast of amine protons on the glutamine molecule undergoing chemical exchange with bulk water. This CEST effect and pH-dependency around amine proton resonance also increased with increasing glutamine concentration (Fig. 1E and F). As the expected amino acid concentration in normal brain is ~20–25 mM,[25] and other similar fast-exchanging amine groups will give rise to additional signal at 3.0 ppm, CEST signal due to these amine protons should be detectable in vivo.

The sigmoidal relationship between MTR_{asym} and pH is suggestive of a cooperative (or inhibitory) exchange process and is consistent with the Bloch–McConnell equations.[26] Interestingly, we observed an apparent contradictory increase in MTR_{asym} at 3.0 ppm with increasing temperature (Fig. 1F); this may be explained by the competing effects from spin-spin relaxation (ie, T2 relaxation rate), which increases with increasing temperature, reducing the line width and increasing the available NMR signal at a given resonant frequency.

Results of the simple competitive inhibitor equation fit suggest no significant difference in the MTR_{asym} at 3.0 ppm for high pH values between the neutral amino acids (Fig. 1G; $P > .05$ for all model parameters), supporting the hypothesis that pH dependence on the amine proton CEST signal may be similar between neutral amino acids with similar chemical composition.

Next, we explored the dependence of MTR_{asym} and pH on the MR scanner field strength. Using Equation 1 to describe the relationship between MTR_{asym} at 3.0 ppm and pH, results suggested that the pH required for 50% of the maximum span in MTR_{asym} at 3.0 ppm between high and low pH limits, or κ, was significantly lower on 1.5T scanners compared with both 3T and 7T, suggesting that 1.5T MR scanners may not provide adequate CEST signal for the range of pH values typically observed in tumors (Fig. 1H; nonlinear regression; κ for 1.5T vs 3T, $P = .0012$ and κ for 1.5T vs 7T, $P = .0440$). Results also suggested that the relationship between MTR_{asym} and pH was similar between 3T and 7T scanners for all parameters besides the CEST asymmetry at high pH, which was slightly lower at 7T (Fig. 1H; Nonlinear regression; α, $P = .7885$; δ, $P = .1166$; κ, $P = .1933$; and β, $P = .0129$). Additionally, results suggested no difference in the actual sensitivity of MTR_{asym} at 3.0 ppm to changes in pH between the 3 field strengths (δ for 1.5T vs 3T, $P = .7924$; δ for 1.5T vs 7T, $P = .1470$, and δ for 3T vs 7T, $P = .1166$) and no differences between the maximum MTR_{asym} at very low pH (α for 1.5T vs 3T, $P = .2311$; α for 3T vs 7T, $P = .7885$; and α for 1.5T vs 7T, $P = .3422$). Together, these results suggest that pH-weighted MRI using endogenous amino acid CEST should be performed at high field strengths in order to ensure adequate contrast for the range of pH values commonly observed in cancer tissues.

We then conducted a series of preclinical pH-weighted MRI experiments at 7T in C57BL/6 mice injected either with PBS (control) or 2×10^4 GL261 glioma cells. Results showed avid contrast enhancement and significantly higher MTR_{asym} (Fig. 1M; paired *t*-test, $P = .0002$; mean MTR_{asym} in tumor = 6.3% vs 3.6% in contralateral tissue) when evaluated at an irradiation frequency of 3.0 ppm offset in tumor, which was not observed in the control animals (Fig. 1I and J). H&E histology confirmed that the areas showing an acidic signature were composed of relatively hypercellular, highly necrotic tumor tissue (Fig. 1K and L).

To demonstrate that CEST contrast at 3.0 ppm is elevated in human brain tumors under conditions where low pH is thought to occur, we assessed a series of high-grade gliomas (WHO III–IV) using pH-weighted MRI, ^{18}F-FDOPA PET, and single-voxel MR spectroscopy. Results demonstrated a positive MTR_{asym} on CEST at 3.0 ppm in regions with elevated ^{18}F-FDOPA PET uptake and elevated lactate concentration (Fig. 2), implying that highly aggressive tumors with elevated amino acid uptake for fuel and increased lactic acid in solution from oncologic metabolism under hypoxic conditions will consistently generate an acidic tumor signature using CEST MRI at 3.0 ppm.

To confirm that regions suspected of containing acidic tissue on pH-weighted MRI contained viable tumor, we performed pH-weighted MR-guided biopsies in 2 patients. The first patient was a 26-year-old male with a large area of T2 hyperintensity, suggestive of tumor, but no contrast enhancement (Fig. 3A and B). ^{18}F-FDOPA PET, perfusion MRI, and diffusion MRI were also negative. An acidic signature consistent with tumor on inferior aspects was shown on pH-weighted MRI (Fig. 3A), whereas superior regions did not demonstrate this signature (Fig. 3B). Biopsy results confirmed that inferior regions contained low-grade glioma tissue with low proliferation rate (Ki-67, ~1%–2%) but high expression of hypoxia-inducible factor-1a, whereas superior regions did not show evidence of tumor. The second patient was a 47-year-old male with suspected recurrent glioblastoma. Upon scanning this patient, pH-weighted MRI suggested extensive acidic tumor regions and elevated ^{18}F-FDOPA uptake confined to areas of enhancement (Fig. 3C). Three biopsies were performed (Fig. 3D), and areas that demonstrated acidic tumor signatures were histologically confirmed to contain recurrent tumor (yellow and red targets), whereas areas lacking CEST contrast at 3.0 ppm (blue target) were shown to contain extensive necrosis and macrophage infiltration consistent with treatment effects. Together, these results suggest pH-weighted MRI using amine CEST may provide high specificity for metabolically active tumor regions.

To test the hypothesis that an acidic microenvironment increases resistance to radiation[12] and chemotherapies[13] in human brain tumors, we performed pH-weighted imaging before, during, and after radiation therapy and temozolomide in

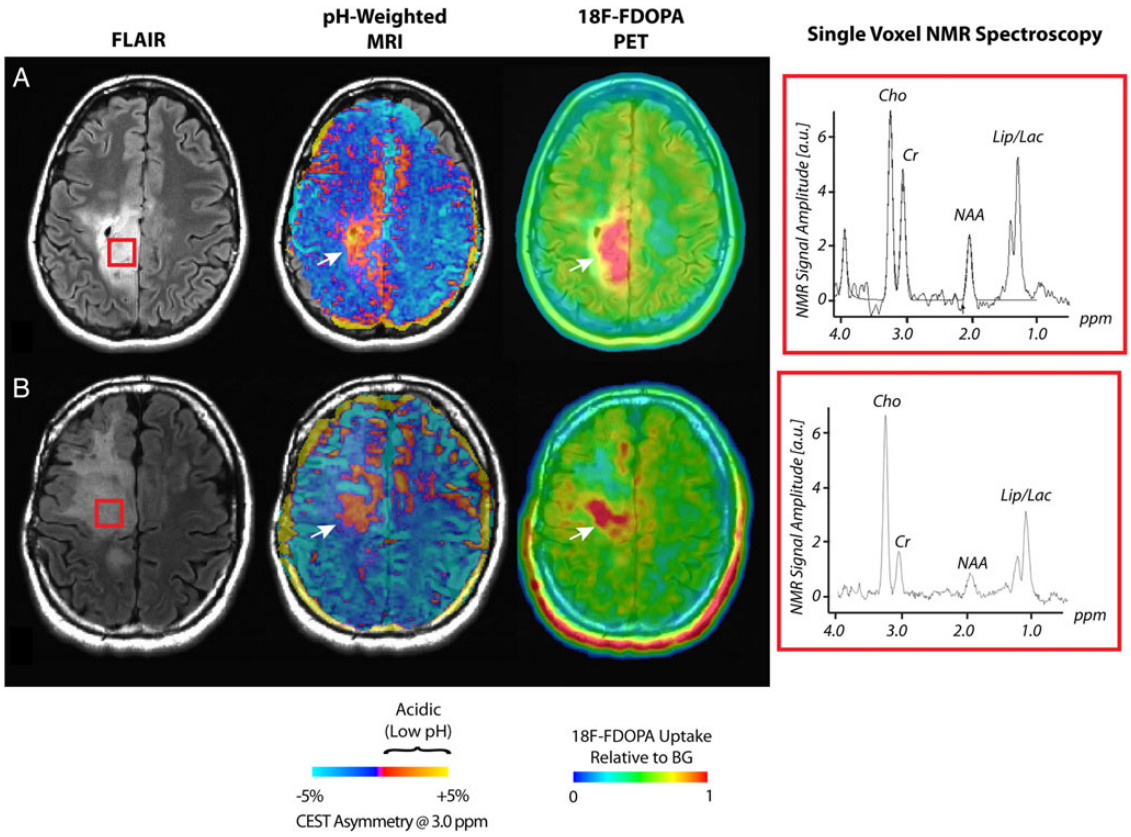

Fig. 2. Spatial correspondence between pH-weighted molecular MRI, ^{18}F-FDOPA PET, and MR spectroscopy. (A and B) Two patients with anaplastic astrocytomas showing CEST asymmetry consistent with low pH in regions with confirmed elevated ^{18}F-FDOPA uptake and lactate. From left to right: T2-weighted FLAIR, pH-weighted MRI using amine CEST, ^{18}F-FDOPA PET, and NMR spectrum from the area shown in the red box in FLAIR images. Cho = choline; Cr = creatine; NAA = N-acetyl aspartate; Lip/Lac = mobile lipids and/or lactate. (Both cases were confirmed to contain lactate based on inversion of the Lip/Lac peak by using an intermediate echo time = 135 ms). BG, basal ganglia.

20 patients with newly diagnosed glioblastoma (Fig. 4) and examined differences in PFS. Patients with tumors that were acidic at baseline following surgical resection but prior to radiation and temozolomide (Fig. 4A), defined by a significant region (>50%) of positive CEST asymmetry at 3.0 ppm within areas of contrast enhancement and/or T2 or FLAIR hyperintensity, demonstrated a significantly longer PFS compared with patients lacking significantly acidic tumors (Fig. 4A–C; log-rank, $P < .0001$; median PFS for acidic tumors vs non-acidic tumors = 125 days vs 450 days). Areas with low pH at baseline often forecasted regions of subsequent tumor growth on contrast-enhanced MRI (Fig. 4A). Although not completely colocalized, examination of CBF maps in these patients confirmed that regions with acidic signatures often occurred in areas of low perfusion, consistent with a high level of hypoxia. Additionally, patients exhibiting an increase in the size of acidic lesions during concurrent radiation and temozolomide (Fig. 4D) had a significantly shorter PFS from the end of radiation therapy compared with tumors exhibiting stable or decreasing acidic lesion size (Fig. 4E; log-rank, $P = .0003$; median PFS in acidic growing tumors = 68 days vs 339 days), implying that acidic tumor size may be useful as an early response biomarker in patients with glioblastoma.

Discussion

Results from the current study support the hypothesis that CEST imaging of the amine protons in solution can be used as a noninvasive pH-weighted MRI technique for human and preclinical investigation of malignant gliomas. CEST MRI provides molecular information about imaging targets that cannot be obtained with standard anatomical imaging techniques. In this study, we quantified the effects of pH and concentration on the CEST signal obtained from the amine functional group, whose protons exchange at a much faster rate (in thousands of Hz) than amide protons in the more commonly used "amide proton transfer," or APT, technique (~30 Hz). CEST contrast as defined by MTR_{asym} at 3.0 ppm was shown to increase with both an increase in amino acid concentration and a decrease in pH within a physiologically relevant pH range for cancer tissues (~6.0 to 7.0 pH). This CEST technique was then implemented in glioblastoma multiforme (GBM) patients to determine whether CEST targeted to the amino acid amine group could provide a pH-weighted biomarker in preclinical models and human tumors.

Although the majority of CEST phantom studies in recent years have targeted proteins or creatine, a select few amino

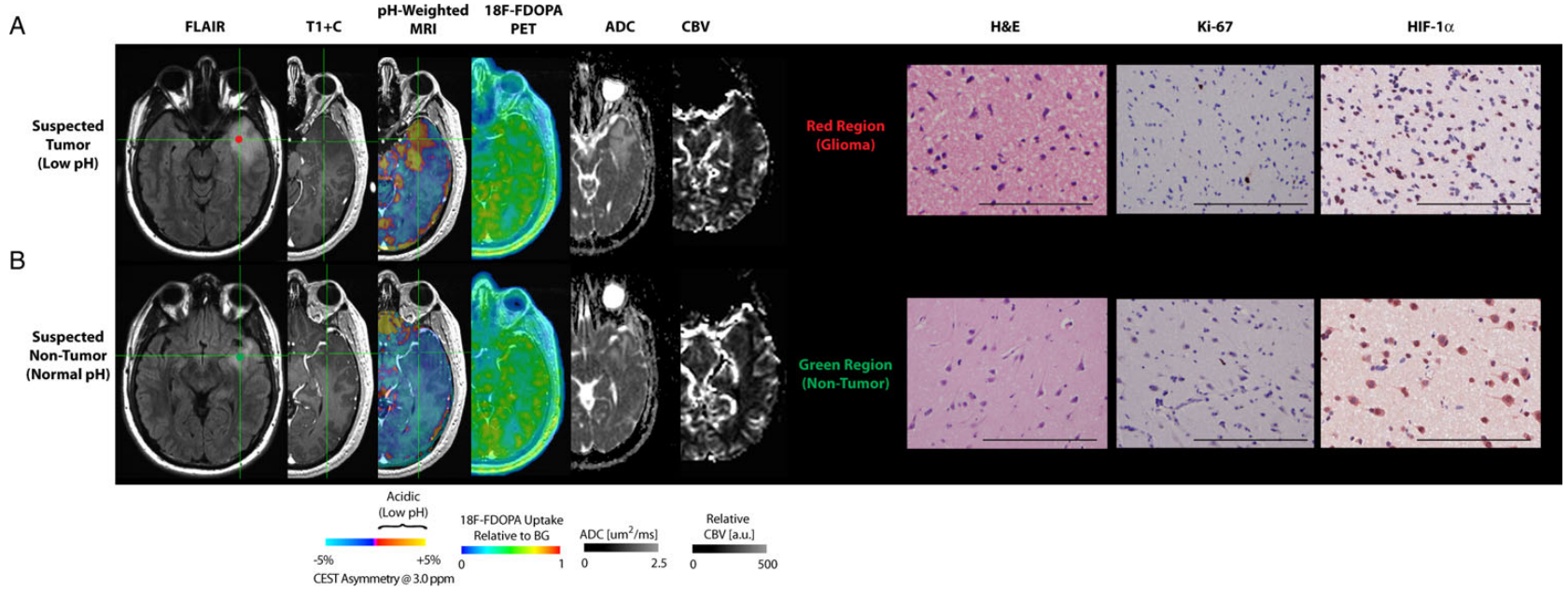

Fig. 3. pH-weighted image-guided biopsies in 2 patients with gliomas. (A and B) A 26-year-old male patient with suspected low-grade glioma (WHO II). FLAIR images show T2 hyperintense regions in the left temporal lobe, but no contrast enhancement on postcontrast T1-weighted images (T1+C) or abnormal ^{18}F-FDOPA PET uptake was observed. Diffusion and perfusion MRI showed on restricted diffusion on apparent diffusion coefficient (ADC) maps and no elevated CBV, respectively. pH-weighted MRI in inferior regions (A) showed elevated CEST asymmetry, consistent with regions of low pH. Superior regions (B), however, did not show CEST asymmetry. Histology for biopsy samples taken from the regions in red (A) were confirmed to contain diffuse astrocytoma cells with low cellularity, low (but present) mitotic figures, and regions of hypoxia. Alternatively, samples obtained from the green region (B) were consistent with hypoxic neurons likely hypertrophied from prolonged seizure activity and lacked mitotic figures or morphologic features of tumor. (C and D) A 47-year-old male patient with recurrent glioblastoma (WHO IV). Postcontrast T1+C demonstrated a large extent of contrast-enhancing tissue suspect of recurrent tumor, but pH-weighted MRI and ^{18}F-FDOPA showed differing areas of abnormality. Three biopsy locations were obtained: yellow = areas of contrast enhancement, avid ^{18}F-FDOPA PET uptake, and low pH on CEST; blue = areas of contrast enhancement, moderate ^{18}F-FDOPA uptake, and normal pH on CEST; red = contrast enhancement, low pH on CEST, and no ^{18}F-FDOPA uptake. Histology from these biopsy sites showed evidence of recurrent glioblastoma with moderate cellularity and focal necrosis in areas of yellow; evidence of treatment effects including macrophages and extensive necrosis in areas of blue; and high tumor cellularity with pseudopalisading necrosis consistent with recurrent glioblastoma in areas of red. Scale bar = 100 μm. BG, basal ganglia.

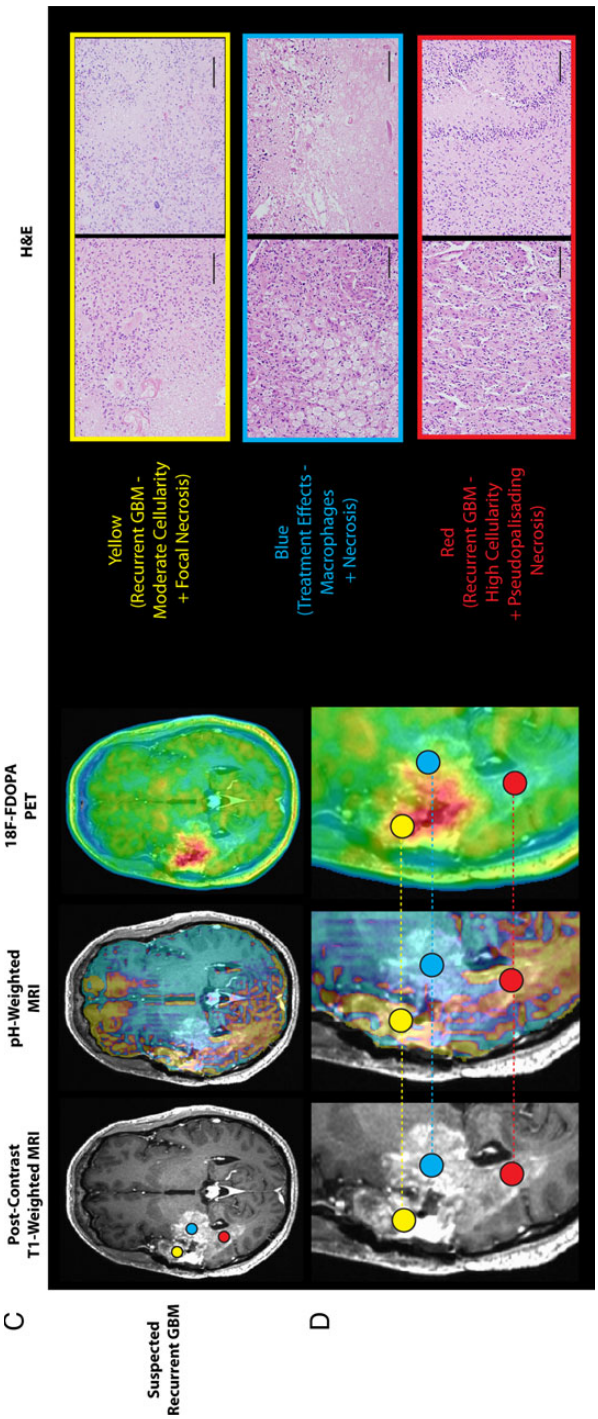

Fig. 3. *Continued*

acids have also been characterized. Cai et al[27] characterized the CEST signature of glutamate phantoms and a rat stroke model at 7T, demonstrating that the CEST signal at 3.0 ppm increases with decreasing pH and increasing concentration, consistent with our findings. In separate studies, Cai et al,[28] Kogan et al,[29] Jin et al,[30] and Jones et al[31] all observed a similar relationship between increasing CEST asymmetry at 3 ppm and decreasing pH at 7T. However, to our knowledge, our study is the first to demonstrate that the CEST signature of amino acid amine protons can be used as pH-weighted contrast at the more common clinical scanner strength of 3T. Additionally, the current study further documents the CEST signatures for additional amino acids, including glycine and phenylalanine, as well as implements an amino acid amine–targeted CEST technique in both preclinical and human brain tumors, which has not been previously reported.

Other studies have explored CEST imaging in human GBM for contrast mechanisms such as APT and nuclear Overhauser enhancement (NOE). For example, Togao et al[32] and Zhou et al[33] showed that APT can stratify patients by tumor grade and differentiate between radiation necrosis and active tumor, respectively. Additionally, Paech et al,[34] Zaiss et al,[35] and Xu et al[36] cleverly exploited the NOE effect at high magnetic fields to show novel contrast within active tumor tissues. These studies, however, were performed at high magnetic field strengths (>7T) where NOE and other contrast mechanisms can influence the underlying CEST signal. Thus, the current study, performed at 3T, appears to provide unique molecular information beyond that of APT or NOE.

While APT imaging has become the most prevalent CEST technique implemented in the clinical setting, the slow exchange rate of the amide protons often necessitates a saturation pulse on the order of seconds to generate sufficient contrast.[37] Targeting the faster exchanging amine protons at 3.0 ppm allows for faster saturation of the target protons and shorter scan times per acquisition compared with APT. Further, APT has been shown to decrease with decreasing pH, making sensitivity to acidic tissue difficult to distinguish from other relaxation mechanisms.[31,38] In comparison, amine CEST effects increase with increasing amino acid concentration and decreasing pH, both conditions that are found in active tumor tissue. However, it is important to note that the increasing effect of amine concentration on the CEST signal only occurs in the presence of a low pH, suggesting that amine CEST may act like a noninvasive "litmus test" for identifying acidic tissues.

There were a few limitations to the current study that should be addressed. As our CEST acquisition contained only a few image slices, we were not able to collect pH-weighted coverage of the full tumor. Future technical improvements to our sequence will allow full brain coverage by leveraging new acceleration techniques. Additionally, the CEST data may be affected by the T2 properties of the tissue in addition to exchange properties, although our identification of hyperintense pH-weighted regions not corresponding to T1 or T2 lesions indicates that mechanisms besides relaxivity are likely responsible for the observed contrast. Finally, although we had 20 patients with serial pH-weighted imaging, we had only 2 patients in which biopsy data were available; a larger cohort of biopsy cases is warranted to correlate histology with pH-weighted imaging.

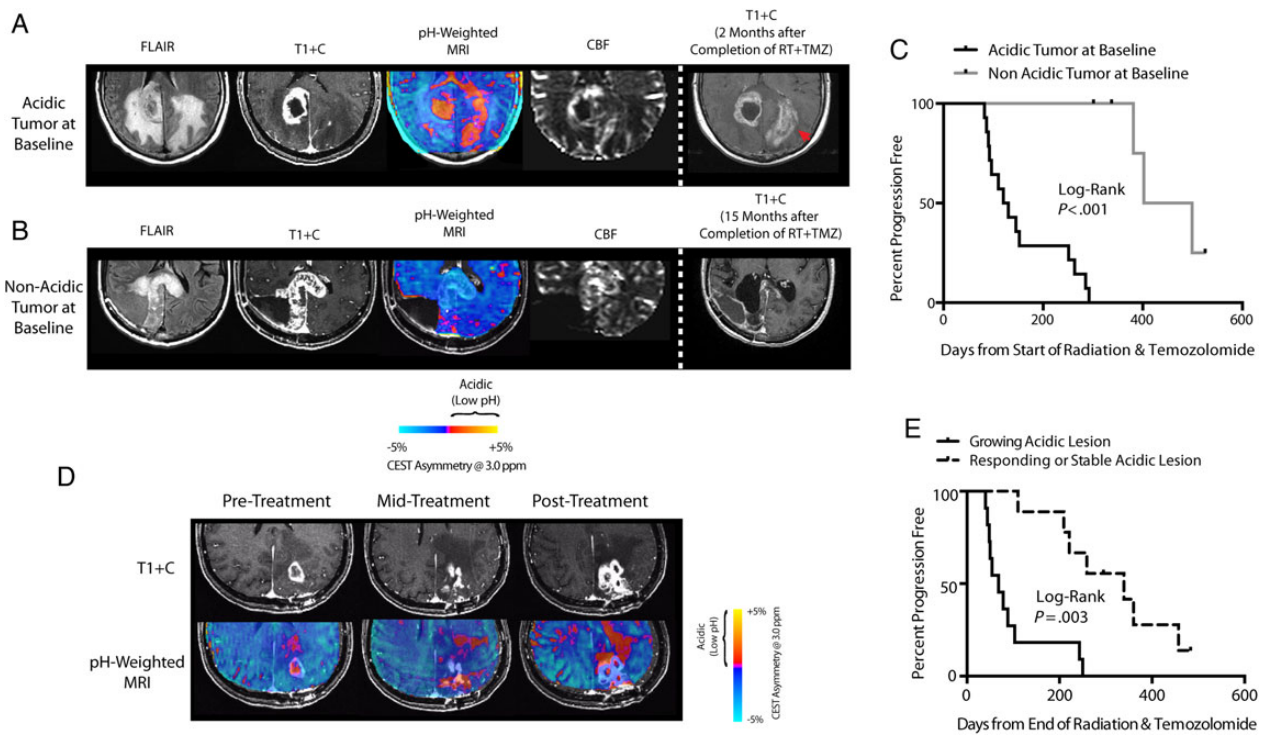

Fig. 4. Acidic tumor response to combination radiochemotherapy. Patients with newly diagnosed glioblastoma ($N = 20$) were evaluated at baseline, following surgery but before combination external beam radiation therapy and temozolomide (A–C), and throughout radiochemotherapy (D–E). (A) A patient with an acidic tumor after surgical resection but prior to radiochemotherapy. CBF maps show elevated perfusion along with pockets of low CBF indicative of hypoxia or edema. Two months after completion of radiochemotherapy, this patient developed contrast enhancement in the left hemisphere, consistent with regions of low pH prior to therapy. (B) A patient with a non-acidic (normal pH) tumor after surgical resection within the corpus callosum. Perfusion MRI showed elevated CBF within the contrast-enhancing portions of the tumor with relatively low CBF in the central necrotic regions. Fifteen months after completion of combination radiochemotherapy, the enhancing tumor reduced more than 40%. (C) Patients with presence of acidic tumor (>50% of the lesion having low pH signal on CEST) had a significantly shorter PFS compared with non-acidic tumors when evaluated prior to radiochemotherapy (log-rank, $P <$ .0001). (D) A patient with acidic tissue within and adjacent to a ring-enhancing lesion in the left hemisphere. During and following combination therapy, this patient demonstrated continually increasing acidic and contrast-enhancing tumor size. (E) Patients with growing acidic lesions had significantly shorter PFS compared with stable or responding acidic lesions (log-rank, $P = .0003$).

Conclusion

Results from the current study support the hypothesis that CEST imaging of the amine protons on glutamine molecules can be used as a noninvasive pH-weighted MRI technique for human and preclinical investigation of malignant gliomas.

Supplementary Materials

Supplementary material is available at Neuro-Oncology Journal online (http://neuro-oncology.oxfordjournals.org/).

Funding

This work was supported by American Cancer Society (ACS) Research Scholar Grant RSG-15-003-01-CCE; NIH/NCI R21CA167354 (BME); a UCLA Jonsson Comprehensive Cancer Center Seed Grant (B.M.E.); a University of California Cancer Research Coordinating Committee Grant (B.M.E.); a Siemens Healthcare Research Grant (B.M.E.); Art of the Brain (T.F.C.); Ziering Family Foundation in memory of Sigi Ziering (T.F.C.); Singleton Family Foundation (T.F.C.); and the Clarence Klein Fund for Neuro-Oncology (T.F.C.).

Conflict of interest statement. No authors have a conflict of interest regarding the current study.

References

1. Gillies RJ. *Causes and Consequences of Acidic pH in Tumors*. West Sussex, UK: John Eiley & Sons, Ltd.; 2001.
2. Wachsberger P, Burd R, Dicker AP. Tumor response to ionizing radiation combined with antiangiogenesis or vascular targeting agents: exploring mechanisms of interaction. *Clin Cancer Res*. 2003;9(6):1957–1971.
3. Raghunand N, Gatenby RA, Gillies RJ. Microenvironmental and cellular consequences of altered blood flow in tumours. *Br J Radiol*. 2003;76 Spec No 1:S11–S22.
4. Warburg O. *The Metabolism of Tumours: Investigations from the Kaiser Wilhelm Institute for Biology*. Berlin-Dahlem, London, UK: Arnold Constable; 1930.

5. Helmlinger G, Sckell A, Dellian M, et al. Acid production in glycolysis-impaired tumors provides new insights into tumor metabolism. *Clin Cancer Res*. 2002;8(4):1284–1291.
6. Gatenby RA, Gillies RJ. Why do cancers have high aerobic glycolysis? *Nat Rev Cancer*. 2004;4(11):891–899.
7. Lardner A. The effects of extracellular pH on immune function. *J Leukoc Biol*. 2001;69(4):522–530.
8. Morita T, Nagaki T, Fukuda I, et al. Clastogenicity of low pH to various cultured mammalian cells. *Mutat Res*. 1992;268(2):297–305.
9. Martinez-Zaguilan R, Seftor EA, Seftor RE, et al. Acidic pH enhances the invasive behavior of human melanoma cells. *Clin Exp Metastasis*. 1996;14(2):176–186.
10. Shi Q, Le X, Wang B, et al. Regulation of vascular endothelial growth factor expression by acidosis in human cancer cells. *Oncogene*. 2001;20(28):3751–3756.
11. Griffiths L, Dachs GU, Bicknell R, et al. The influence of oxygen tension and pH on the expression of platelet-derived endothelial cell growth factor/thymidine phosphorylase in human breast tumor cells grown in vitro and in vivo. *Cancer Res*. 1997;57(4):570–572.
12. Freeman ML, Sierra E. An acidic extracellular environment reduces the fixation of radiation damage. *Radiat Res*. 1984;97(1):154–161.
13. Reichert M, Steinbach JP, Supra P, et al. Modulation of growth and radiochemosensitivity of human malignant glioma cells by acidosis. *Cancer*. 2002;95(5):1113–1119.
14. Sun PZ, Benner T, Copen WA, et al. Early experience of translating pH-weighted MRI to image human subjects at 3 Tesla. *Stroke*. 2010;41(10 Suppl):S147–S151.
15. Souba WW. Glutamine and cancer. *Ann Surg*. 1993;218(6):715–728.
16. Kovacevic Z, Morris HP. The role of glutamine in the oxidative metabolism of malignant cells. *Cancer Res*. 1972;32(2):326–333.
17. Medina MA, Sanchez-Jimenez F, Marquez J, et al. Relevance of glutamine metabolism to tumor cell growth. *Mol Cell Biochem*. 1992;113(1):1–15.
18. Schmitt B, Zaiss M, Zhou J, et al. Optimization of pulse train presaturation for CEST imaging in clinical scanners. *Magn Reson Med*. 2011;65(6):1620–1629.
19. Wen PY, Macdonald DR, Reardon DA, et al. Updated response assessment criteria for high-grade gliomas: response assessment in neuro-oncology working group. *J Clin Oncol*. 2010;28(11):1963–1972.
20. Schmainda KM, Rand SD, Joseph AM, et al. Characterization of a first-pass gradient-echo spin-echo method to predict brain tumor grade and angiogenesis. *AJNR Am J Neuroradiol*. 2004;25(9):1524–1532.
21. Boxerman JL, Schmainda KM, Weisskoff RM. Relative cerebral blood volume maps corrected for contrast agent extravasation significantly correlate with glioma tumor grade, whereas uncorrected maps do not. *AJNR Am J Neuroradiol*. 2006;27(4):859–867.
22. Kim M, Gillen J, Landman BA, et al. Water saturation shift referencing (WASSR) for chemical exchange saturation transfer (CEST) experiments. *Magn Reson Med*. 2009;61(6):1441–1450.
23. Kinahan PE, Townsend DW, Beyer T, et al. Attenuation correction for a combined 3D PET/CT scanner. *Med Phys*. 1998;25(10):2046–2053.
24. Nuyts J, Michel C, Dupont P. Maximum-likelihood expectation-maximization reconstruction of sinograms with arbitrary noise distribution using NEC-transformations. *IEEE Trans Med Imaging*. 2001;20(5):365–375.
25. Perry TL, Hansen S, Berry K, et al. Free amino acids and related compounds in biopsies of human brain. *J Neurochem*. 1971;18(3):521–528.
26. McConnell HM. Reaction rates by nuclear magnetic resonance. *J Chem Phys*. 1958;28(3):430–431.
27. Cai K, Haris M, Singh A, et al. Magnetic resonance imaging of glutamate. *Nat Med*. 2012;18(2):302–306.
28. Cai K, Singh A, Roalf DR, et al. Mapping glutamate in subcortical brain structures using high-resolution GluCEST MRI. *NMR Biomed*. 2013;26(10):1278–1284.
29. Kogan F, Singh A, Debrosse C, et al. Imaging of glutamate in the spinal cord using GluCEST. *Neuroimage*. 2013;77:262–267.
30. Jin T, Wang P, Zong X, et al. Magnetic resonance imaging of the amine-proton exchange (APEX) dependent contrast. *Neuroimage*. 2012;59(2):1218–1227.
31. Jones CK, Huang A, Xu J, et al. Nuclear Overhauser enhancement (NOE) imaging in the human brain at 7T. *Neuroimage*. 2013;77:114–124.
32. Togao O, Yoshiura T, Keupp J, et al. Amide proton transfer imaging of adult diffuse gliomas: correlation with histopathological grades. *Neuro Oncol*. 2014;16(3):441–448.
33. Zhou J, Tryggestad E, Wen Z, et al. Differentiation between glioma and radiation necrosis using molecular magnetic resonance imaging of endogenous proteins and peptides. *Nat Med*. 2011;17(1):130–134.
34. Paech D, Zaiss M, Meissner JE, et al. Nuclear overhauser enhancement mediated chemical exchange saturation transfer imaging at 7 Tesla in glioblastoma patients. *PLoS One*. 2014;9(8):e104181.
35. Zaiss M, Windschuh J, Paech D, et al. Relaxation-compensated CEST-MRI of the human brain at 7T: unbiased insight into NOE and amide signal changes in human glioblastoma. *Neuroimage*. 2015;112:180–188.
36. Xu J, Zaiss M, Zu Z, et al. On the origins of chemical exchange saturation transfer (CEST) contrast in tumors at 9.4T. *NMR Biomed*. 2014;27(4):406–416.
37. McMahon MT, Gilad AA, Zhou J, et al. Quantifying exchange rates in chemical exchange saturation transfer agents using the saturation time and saturation power dependencies of the magnetization transfer effect on the magnetic resonance imaging signal (QUEST and QUESP): pH calibration for poly-L-lysine and a starburst dendrimer. *Magn Reson Med*. 2006;55(4):836–847.
38. McVicar N, Li AX, Goncalves DF, et al. Quantitative tissue pH measurement during cerebral ischemia using amine and amide concentration-independent detection (AACID) with MRI. *J Cereb Blood Flow Metab*. 2014;34(4):690–698.